Volume 1 | Number 1 | Jan 2013 | Pages 1–100

ChemComm

Chemical Communications
www.rsc.org/chemcomm

ROYAL SOCIETY OF CHEMISTRY

ROYAL SOCIETY OF CHEMISTRY

www.rsc.org/chemcomm

Journal Name

COMMUNICATION

Ultrathin HNbWO$_6$ Nanosheets: Facile Synthesis and Enhanced Hydrogen Evolution Performance from Photocatalytic Water Splitting

Yuhao Liu, Jinhua Xiong, Shuiguang Luo, Ruowen Liang, Na Qin, Shijing Liang*, Ling Wu*

Ultrathin monolayer HNbWO$_6$ nanosheets have been successfully prepared through a simple and ultrafast ion intercalation assisted exfoliation method. These obtained highly dispersed nanosheets present enhanced photocatalytic hydrogen evolution activity than the prepared nanosheets by the traditionally time-consuming process.

Since the physical exfoliation of graphite into merely one carbon atom thick graphene single sheets, this discovery has triggered exponential growth of research and development into this fascinating ultrathin nanomaterials.[1] These single sheets, so-called nanosheets, can be regarded as a new class of materials, which have extremely small thickness of ~1 nm and are up to several tens of micrometers in lateral size.[2, 3] Particularly, ultrathin metal oxide nanosheets have drawn tremendous attention owing to their various elemental composition and distinctive properties, such as high surface area, anisotropic features, and single-crystalline texture.[4-6] The unique characteristics of these nanostructures make them as functional materials including cosmetics,[7] optoelectronics[8] and heterogeneous photocatalysis.[9-12] More importantly, the single molecular layers of these materials provide a chance for understanding the photocatalytic reaction on a molecular level.[13, 14]

Generally, the effective approach of synthesis two-dimensional (2D) nanosheets can be divided into two major categories: "top–down" and "bottom–up" methods according to the processes of creating nanoscale structures.[15-18] Up to now, several ultrathin metal oxides nanostructures have been prepared by a bottom-up approach through either the vapor deposition method[19] or wet-chemical one-pot synthesis,[20, 21] but this approach need to seek the molecular or atomic components to built more complex nanoscale assemblies or directed self-assemblies based on complex mechanisms and technologies.[22, 23] Therefore, ultrathin nanosheets mainly prepared by a much more mild top–down approach through ion-exchange, intercalation, swelling, mechanical shaking and subsequent reassembly processes.[24, 25] However, this type of exfoliation is considered to be time-consuming owing to slow diffusion processes and takes typically 1–2 weeks according to

several reports.[26] In view of this, it is necessary to develop a very rapid and time-efficient approach for the preparation of 2D metal oxides nanosheets.

Herein, we report an efficient, simple method towards the ultrafast synthesis of ultrathin metal oxides nanosheets based on an acid–base reaction and ion intercalation assisted exfoliation strategy. Simply, dispersing the layered parent of HNbWO$_6$•1.5H$_2$O in the polar amine of triethanolamine aqueous solution, then a translucent colloidal nanosheets suspensions can be obtained in just a few minutes. Scheme 1 illustrates the procedure for the fabrication of 2D ultrathin HNbWO$_6$ nanosheets. It is found that the obtained well-dispersed ultrathin monolayer HNbWO$_6$ nanosheets suspensions exhibit an efficient photocatalytic H$_2$ evolution performance by in-situ reaction under simulated sunlight irradiation. Moreover, highly dispersed and hyperfine Pt nanoparticles loading on the ultrathin HNbWO$_6$ nanosheets via in-situ photodepositon method showed a remarkable promotion for photocatalytic hydrogen production.
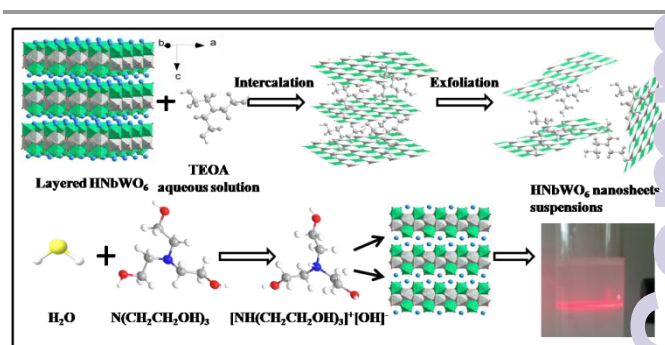
Scheme 1 Scheme illustrating the preparation of ultrathin HNbWO$_6$ nanosheets through the acid–base reaction and ion intercalation assisted exfoliation strategy.

Monolayer HNbWO$_6$ nanosheets suspensions were synthesized rapidly using triethanolamine (TEOA) (see ESI for details). The samples are denoted as N-HNbWO$_6$. Restacked HNbWO$_6$ nanosheets aggregates synthesized by the traditional approach with tetra-n-butylammonium hydroxide (TBAOH) are denoted as T-

HNbWO$_6$. Structural analysis of the synthetic samples was carried out by XRD (Fig. S1). The single-phase diffraction pattern of layered LiNbWO$_6$ and HNbWO$_6$ samples matches well with the published data (JCPDS: 41-0378 and 41-0110, respectively). The characteristic (002) peak shifted to a lower 2θ angle after the proton-exchange process, indicating that the interlayer distance of HNbWO$_6$ (d=1.30 nm) is wider than that of LiNbWO$_6$ (d=0.93 nm). This will benefit the intercalation of organic base in a subsequent exfoliation process. Compared with the layered parent compounds, HNbWO$_6$ nanosheets obtained by this rapid acid–base reaction method with TEOA aqueous solution lost their periodic layered structure and long-range order characteristics in c axial, only showing a few weak in-plane diffraction peaks of (110), (200) and (220).[15] Owing to the disorder restacking, the (002) peak further shifted to lower 2θ at 6.34°. These results are consistent with the T-HNbWO$_6$ nanosheets.
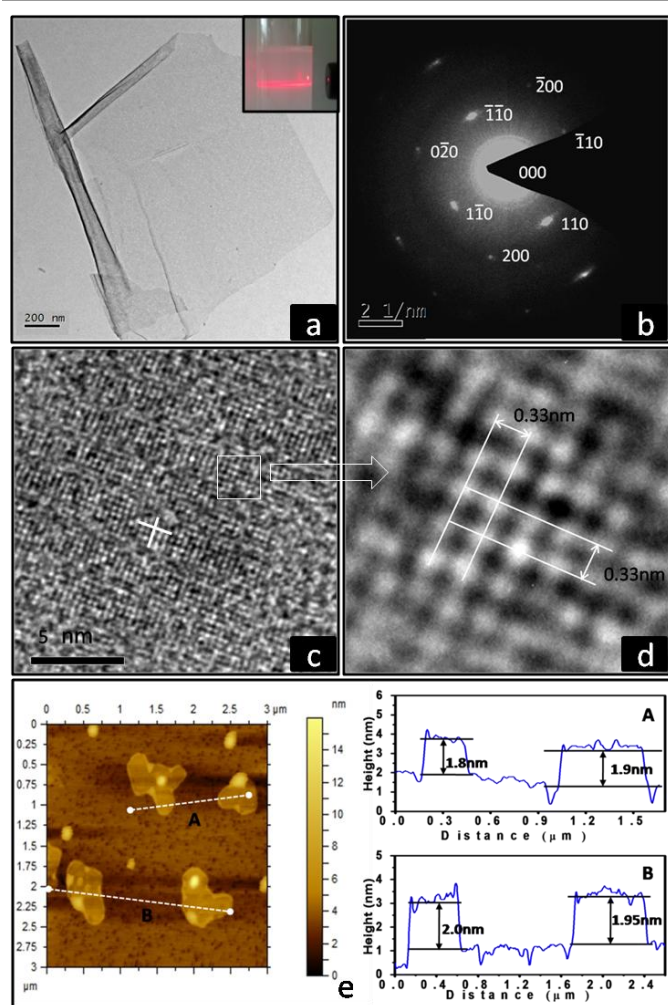

Fig. 1 (a) TEM images of ultrathin HNbWO$_6$ nanosheets suspensions. The inset in (a) is the photograph of the colloidal HNbWO$_6$ nanosheets dispersions. The light beam is incident from the side to demonstrate the Tyndall effect. (b) SAED and (c) HRTEM image taken from a part of a single nanosheet. (d) HRTEM image enlarge from (c). (e) Representative AFM image (left) and corresponding thickness analysis (right) taken around the white line in left.

A typical layer structure of LiNbWO$_6$ and HNbWO$_6$ was observed stacked layer by layer from the SEM in Fig S2a and Fig 2b,

respectively. These layered metal oxides consist of tabular particles in size of 3-20 μm, while the thickness of layered HNbWO$_6$ flakes is about 50 nm. The image of the HNbWO$_6$ nanosheets prepared by this rapid acid–base reaction method indicate that the formation random aggregation of rather loose and irregular 2D nanosheets (Fig. S2c).[27] This image is similar to the nanosheets obtained by traditional method (Fig. S2d). The morphology of these rapid synthesized nanosheets was further confirmed by TEM and HRTEM images (Fig. 1). The individual sheets obtained by this approach (Fig. 1a), with edge lengths of several hundred nanometers. Note that in the edge of nanosheets, nanotubes were formed by the rolling up of exfoliated HNbWO$_6$ nanosheets. The produced nanotubes were usually 40–50 nm in diameter and several hundred nanometers in length.[28] The difference of chemical exfoliation reagents caused the cooperative distortion of MO$_6$ octahedral in HNbWO$_6$ might become a source of internal stress and induce the rolling-up behavior.[29, 30] The HNbWO$_6$ nanosheets suspensions obtained by this method has obvious Tyndall effect in Fig. 1a, insert, indicating the formation of freestanding and homogeneous 2D ultrathin nanosheets. As shown in Fig. 1b, the SAED analysis on an individual nanosheet reveals some bright spots of the single crystalline feature, which can be indexed as the [001] zone axis of the tetragonal lattice in planar orientation. The HRTEM image (Fig. 1c) shows the clear lattice image, which demonstrates that HNbWO$_6$ nanosheets retain the high in-plane crystallinity. The angle labeled in the enlarged HRTEM image (Fig. 1d) is 90°, which is in agreement with the theoretical value of the angle between the (010) and (100) planes. The clear fringes with lattice spacing are 0.33nm, which corresponds to the (110) plane of tetragonal HNbWO$_6$. Visualization of the nanosheets can be realized by Atomic force microscopy (AFM) in Fig. 1e, exfoliated nanosheets with a lateral size in the range of submicrometers, most of the measured thickness of single layer HNbWO$_6$ nanosheets is between 1.8 and 2.0 nm. This result is well matched with the expected value of the thickness of HNbWO$_6$ layer (Fig. S3), indicating that the as-prepared HNbWO$_6$ nanosheets were monolayer. The difference between experimental height and slab thickness might arise from the distortion of monolayer nanosheet and the adsorption of triethanolamine molecules and water molecules on the surface of nanosheets (see Fig. S4). Such behavior was in accordance with previous results in oxide nanosheets systems.[31, 32]

In addition, the energy dispersive X-ray spectrometry (EDS) analysis was conducted to confirm the composition of these HNbWO$_6$ nanosheets (Fig. S5a). The elements, Nb, W and O were all detected. The EDS mapping in Fig S5b clearly shows that the strong signals for Nb, W and O, further confirming that this method is an effective and fast method for preparing ultrathin nanosheets. In conclusion, the above mentioned results provide direct and solid evidence to the formation of monolayer HNbWO$_6$ nanosheets. For comparison, the TEM and AFM of HNbWO$_6$ nanosheets prepared by traditional method with TBAOH aqueous solution was also shown in Fig S6a and Fig S6b, respectively. All these results indicate that this method has advantage than the traditional approach for the

COMMUNICATION

preparation of monolayer $HNbWO_6$ nanosheets. The introduction of TEOA as a stripping agent based on an acid–base reaction and ion intercalation process is a key factor that promotes the exfoliation of the layered precursors. It is believed that the amine end of the TEOA tends to accept a proton from water because of the presence of lone electron pairs, generating $[HN(CH_2CH_2OH)_3]^+[OH]^-$, which can passively diffuse between the two regions along with the H^+ and OH^-. The in situ information of $[HN(CH_2CH_2OH)_3]^+[OH]^-$ between the neighboring layers offering this layered material for stripping.[33-35] We also demonstrated that this method was suitable to obtain $HNbxTa1-xWO_6$ (x=0.7, 0.5, 0.3, 0) ultrathin nanosheets (see Fig. S7), suggesting the generality of the protocol. In addition, the stripping agent can also replace with other polar amines of Triisopropanolamine (TIPA) for efficient and ultrafast preparation of ultrathin $HNbWO_6$ nanosheets (see Fig. S8).
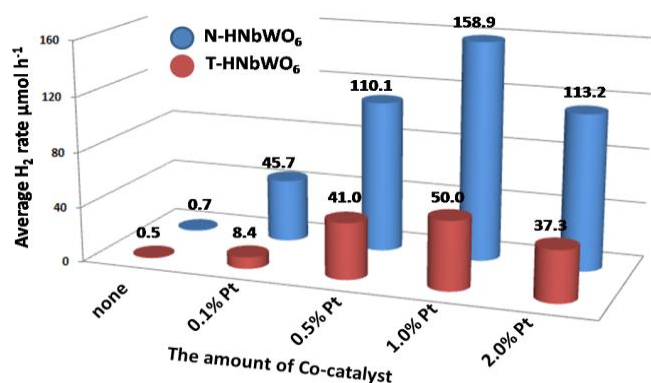

Fig. 2 Average H_2 evolution rate of N-$HNbWO_6$ and T-$HNbWO_6$ loaded with different amount of Pt co-catalyst reaction for five hours.

The BET surface area of restacked $HNbWO_6$ nanosheets prepared by TEOA and TBAOH aqueous solution is about 41.4 and 84.5 m^2g^{-1}, respectively, which is larger than that of layered $HNbWO_6$ (10.7 m^2g^{-1}). The adsorption–desorption isotherm of nanosheets is a type IV isotherm, whereas the layered $HNbWO_6$ displays a type II isotherm (Fig. S9a). The pore size distribution of restacked nanosheets mainly ranges from 0.1 to 30 nm (Fig. S9b), suggesting that the as-exfoliated $HNbWO_6$ maintains the free-standing nanosheets form. The band gap energy and electronic properties of prepared nanosheets were calculated from UV–vis diffuse reflectance spectra and Mott–Sckottky measurements, respectively. As shown in Fig. S10, the flat-band potential of N-$HNbWO_6$, T-$HNbWO_6$ and L-$HNbWO_6$ was ca. −0.88 V, −0.84 V and -0.94V vs Ag/AgCl at pH=6.8, respectively, corresponding to ca. −0.68 V, −0.64 V and -0.74V vs NHE at pH=6.8, respectively, which is more negative than the H_2O/H_2 potential (-0.41 V vs NHE at pH=6.8). Therefore, it is thermodynamically permissible for the transformation of photogenerated electrons to the H_2O to produce H_2.

Using these highly dispersed monolayer $HNbWO_6$ nanosheets suspensions as heterogeneous photocatalysts, H_2 evolution

reactions were conducted under simulated sunlight irradiation. (Fig. S11). For comparison, the photocatalytic performances of restacked $HNbWO_6$ nanosheets obtained with TBAOH were further evaluated by redispersion them in the TEOA aqueous solution. As presented Fig. 2, N-$HNbWO_6$ and T-$HNbWO_6$ show negligible activity for hydrogen evolution without Pt modification. In contrast, the activity of them both improved remarkably with the Pt loading due to the Schottky barrier junctions. Moreover, the average hydrogen production rate of N-$HNbWO_6$ is strikingly higher than T-$HNbWO_6$. The reduction in activity of T-$HNbWO_6$ could be attributed to a mild blockage of surface sites by the adsorption of bulkier TBA^+ cations.[26] TEM of restacked $HNbWO_6$ nanosheets (Fig. S12) also further confirmed that these aggregates were comprised of irregularly stacked and folded nanosheets, no single sheets were observed. Furthermore, the hydrogen production amount of 1.0 wt % Pt loaded N-$HNbWO_6$ was up to 794.5 μmol for five hours (with stable H_2 evolution rate of 158.9 μmol h^{-1}), which was much higher than that of T-$HNbWO_6$ (Fig. S13). The apparent quantum yield of 1.0 wt% Pt loaded N-$HNbWO_6$ and T-$HNbWO_6$ was 14.1% and 2.4%, respectively (Fig. S14).
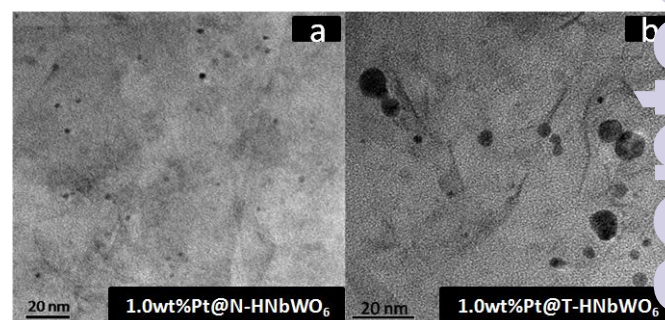

Fig. 3 TEM images of 1.0 wt % Pt loaded N-$HNbWO_6$ (a) and T-$HNbWO_6$ nanosheets (b)

In heterogeneous photocatalysis, the size and uniformity of co-catalyst significant impact on the photocatalytic water splitting performance, the smaller size and highly dispersed of cocatalyst particles are more active for H_2.[36, 37] From Fig. 3a and 3b, the Pt nanoparticles anchored on these nanosheets suspensions were smaller and more dispersed, while some Pt particles agglomerates were formed on the restacked T-$HNbWO_6$ nanosheets. Thus, the enhancement of the photocatalytic activity of the well-dispersed ultrathin monolayer nanosheets suspensions may be attributed to these $HNbWO_6$ nanosheets suspensions are more easily dispersed Pt nanoparticles than restacked nanosheets aggregates, at the same time the particle size of Pt nanoparticles anchored on this nanosheets suspensions are smaller. ICP results show that the percentage of Pt in the sample N-$HNbWO_6$ and T-$HNbWO_6$ was 0.93% and 0.92%, respectively, further revealing that the difference of the activities between these two samples was not caused by the different content of Pt loading. All these results indicate that highly dispersed and hyperfine Pt nanoparticles were key factors for the enhanced photocatalytic H_2 production activity of the N-$HNbWO_6$.

In summary, ultrathin $HNbWO_6$ nanosheets have been successfully obtained via an ultrafast, simple and efficient

exfoliation method based on an acid–base reaction and ion intercalation strategy. The as-prepared $HNbWO_6$ ultrathin nanosheets suspensions are stable and highly dispersed. Compared the $HNbWO_6$ nanosheets aggregates prepared by TBAOH aqueous solution, These ultrathin $HNbWO_6$ nanosheets suspensions showed efficient activity for photocatalytic H_2 evolution, due to the in-situ deposition of smaller and highly dispersed noble-metal clusters. We believe that our strategy could be broadly applicable for the facile production of other ultrathin nanostructures with great promise for various applications.

Acknowledgements

Notes and references

1   K. S. Novoselov, A. K. Geim, S. Morozov, D. Jiang, Y. Zhang, S. a. Dubonos, I. Grigorieva and A. Firsov, *Science*, 2004, **306**, 666-669.
2   T. Shibata, G. Takanashi, T. Nakamura, K. Fukuda, Y. Ebina and T. Sasaki, *Energy Environ. Sci.*, 2011, **4**, 535-542.
3   L. Wang and T. Sasaki, *Chem. Rev.*, 2014, **114**, 9455-9486.
4   S. I. Shin, A. Go, I. Y. Kim, J. M. Lee, Y. Lee and S.-J. Hwang, *Energy Environ. Sci.*, 2013, **6**, 608-617.
5   M. Xu, T. Liang, M. Shi and H. Chen, *Chem. Rev.*, 2013, **113**, 3766-3798.
6   S. Z. Butler, S. M. Hollen, L. Cao, Y. Cui, J. A. Gupta, H. R. Gutierrez, T. F. Heinz, S. S. Hong, J. Huang and A. F. Ismach, *ACS nano*, 2013, **7**, 2898-2926.
7   A. López-Galindo, C. Viseras and P. Cerezo, *Appl. Clay Sc.*, 2007, **36**, 51-63.
8   M. Osada and T. Sasaki, *Adv. Mater.*, 2012, **24**, 210-228.
9   T. W. Kim, S. G. Hur, S.-J. Hwang, H. Park, W. Choi and J.-H. Choy, *Adv. Funct. Mater.,* 2007, **17**, 307.
10 J. L. Gunjakar, T. W. Kim, H. N. Kim, I. Y. Kim and S.-J. Hwang, *J. Am. Chem. Soc.*, 2011, **133**, 14998-15007.
11 K. Maeda, M. Eguchi, W. J. Youngblood and T. E. Mallouk, *Chem. Mater.*, 2009, **21**, 3611-3617.
12 Y. Okamoto, S. Ida, J. Hyodo, H. Hagiwara and T. Ishihara, *J. Am. Chem. Soc.*, 2011, **133**, 18034-18037.
13 J. MeurigáThomas, *Chem. Commun.*, 2006, 3273-3278.
14 S. Liang, L. Wen, S. Lin, J. Bi, P. Feng, X. Fu and L. Wu, *Angew. Chem.*, 2014, **126**, 2995-2999.
15 T. Sasaki and M. Watanabe, *J. Am. Chem. Soc.,* 1998, **120**, 4682-4689.
16 F. Geng, R. Ma, Y. Yamauchi and T. Sasaki, *Chem. Commun.*, 2014, **50**, 9977-9980.
17 M. A. Bizeto, A. L. Shiguihara and V. R. Constantino, *J. Am. Chem. Soc.,* 2009, **19**, 2512-2525.
18 Z. Zhai, C. Hu, X. Yang, L. Zhang, C. Liu, Y. Fan and W. Hou, *J. Mater. Chem.*, 2012, **22**, 19122-19131.
19 T. Orzali, M. Casarin, G. Granozzi, M. Sambi and A. Vittadini, *Phy. Rev. Lett.*, 2006, **97,** 156101.
20 E. L. Tae, K. E. Lee, J. S. Jeong and K. B. Yoon, *J. Am. Chem. Soc.*, 2008, **130**, 6534-6543.
21 S. Liang, S. Zhu, Y. Chen, W. Wu, X. Wang and L. Wu, *J. Mater. Chem.*, 2012, **22**, 2670-2678.
22 K. Sakakibara, J. P. Hill and K. Ariga, *Small*, 2011, **7**, 1288-1308.
23 S. Acharya, J. P. Hill and K. Ariga, *Adv. Mater.*, 2009, **21**, 2959-2981.
24 T. Sasaki, M. Watanabe, H. Hashizume, H. Yamada and H. Nakazawa, *Chem. Commun.*, 1996, 229-230.
25 M. Leng, Y. Chen and J. Xue, *Nanoscale*, 2014, **6**, 8531-8534.
26 K. Nakagawa, T. Jia, W. Zheng, S. M. Fairclough, M. Katoh, S. Sugiyama and S. C. E. Tsang, *Chem. Commun.*, 2014, **50**, 13702-13705.
27 C. Hu, L. Zhang, L. Cheng, J. Chen, W. Hou and W. Ding, J. *Energy. Chem.*, 2014, **23**, 136-144.
28 P. Liu, H. Zhang, H. Liu, Y. Wang, X. Yao, G. Zhu, S. Zhang and H. Zhao, *J. Am. Chem. Soc.,* 2011, **133**, 19032-19035.
29 R. E. Schaak and T. E. Mallouk, *Chem. Mater.*, 2000, **12**, 3427-3434.
30 G. B. Saupe, C. C. Waraksa, H.-N. Kim, Y. J. Han, D. M. Kaschak, D. M. Skinner and T. E. Mallouk, *Chem. Mater.*, 2000, **12**, 1556-1562.
31 P. Shen, H. Zhang, H. Liu, J. Xin, L. Fei, X. Luo, R. Ma and S. Zhang, *J. Mater. Chem. A*, 2015, **3**, 3456-3464.
32 K. Akatsuka, G. Takanashi, Y. Ebina, M.-a. Haga and T. Sasaki, *J. Phys. Chem. C*, 2012, **116**, 12426-12433.
33 F. Geng, R. Ma, A. Nakamura, K. Akatsuka, Y. Ebina, Y. Yamauchi, N. Miyamoto, Y. Tateyama and T. Sasaki, *Nat. commun.*, 2013, **4**, 1632.
34 F. Geng, R. Ma, Y. Ebina, Y. Yamauchi, N. Miyamoto and T. Sasaki, *J. Am. Chem. Soc.,* 2014, **136**, 5491-5500.
35 H. Yuan, D. Dubbink, R. Besselink and J. E. ten Elshof, *Angew. Chem. Int. Ed.*, 2015.
36 E. M. Sabio, R. L. Chamousis, N. D. Browning and F. E. Osterloh, *J. Phys. Chem. C*, 2012, **116**, 3161-3170.
37 T. Oshima, D. Lu, O. Ishitani and K. Maeda, *Angew. Chem. Int. Ed.*, 2015, **54**, 2698-2702.